VALIDATION OF A TURBULENT BOUNDARY LAYER METHOD FOR FUSELAGES OF HELICOPTERS

Hilal Inac, German Aerospace Center (DLR), Institute of Aerodynamics and Flow Technology, Braunschweig, Germany
Thorsten Schwarz, German Aerospace Center (DLR), Institute of Aerodynamics and Flow Technology, Braunschweig, Germany

Abstract

The flow field over a helicopter is exceedingly complex due to various aerodynamic phenomena occurring simultaneously. The precise calculation of the boundary layer in three-dimensional, viscous flow is an old und repeatedly sought-after goal in helicopter aerodynamics. Panel methods calculate frictionless flows including interference effects through potential flow assumption with good accuracy. Since viscous drag cannot be predicted with panel methods alone, the panel methods have to be coupled with a boundary layer method. This paper describes the newly implemented Truckenbrodt's boundary layer method for helicopter fuselages in DLR's unsteady 3D panel and free-wake code UPM, with the aim of improving friction forces and flow separation prediction accuracy. The focus of this paper is to validate the implementation with experimental wind tunnel results of the DLR-internal project Fast Rescue. As an application example, UPM is used to simulate the aerodynamics of a medical personnel deployment vehicle. The results show that the boundary layer method is able to provide reasonable force and moment coefficients and identify flow separation regions.

1. NOTATION

Symbols

c_f	Skin friction coefficient, -
c_p	Pressure coefficient, -
E_3	Integration constant, -
G	Parameter, -
H	Form factor, -
Re	Reynolds number, -
s	Arc length, m
U	Velocity distribution of the flow, m/s
N	Parameter, -
α	Angle of attack, deg
β	Angle of yaw, deg
δ_1	Displacement thickness, m
δ_2	Momentum boundary layer thickness, m
δ_3	Energy loss thickness, m
ν	Kinematic velocity, m^2/s

Acronyms:

BL	Boundary layer
CFD	Computational Fluid Dynamics
CPACS	Common Parametric Aircraft Configuration Scheme
DNW	German Dutch Wind Tunnels
ERF	European Rotorcraft Forum
IRIS	Integrated Rotorcraft Initial Sizing
NWB	Low speed Wind-Tunnel Braunschweig
UPM	Unsteady Panel Method

2. INTRODUCTION

Viscous effects like attached boundary layers and separated flow are very strong on helicopter fuselages. Typical regions for flow separations are, for example, retreating blade stall or massive flow separations on blunt fuselage shapes. Since viscous effects cause friction forces, pressure drag and may cause lift breakdown, it is of great importance to consider viscous effects in numerical prediction tools. Many approximate methods have been developed to resolve the boundary layer close to the surface. Goldschmied's method, Head's method, Cebeci-Smith method (Ref. 3) or Stratford's method (Ref. 11) are the example methods used for turbulent flows. Furthermore, the CFD (Computational Fluid Dynamics) method is an established high-fidelity numerical method where viscous effects are inherently considered when solving the Navier-Stokes equations and using a turbulence model. The flow calculations with CFD are more accurate compared to boundary layer methods but the computational effort is significantly higher. In contrast, low-fidelity aerodynamic codes relying on tabulated aerodynamic data like blade element theory included in comprehensive codes are faster but these methods do not deliver results about the flow on surfaces. In opposition to comprehensive codes, mid-fidelity panel methods consider interference effects and deliver results about the surfaces while the simulation effort is considerably lower than for CFD. Panel methods calculate frictionless flows including interference effects robustly through potential flow assumption. But the mid-fidelity panel methods require the explicit modeling of viscous effects with boundary layer methods. UPM (Unsteady Panel Method) (Ref 15) is a mid-fidelity panel-freewake method developed by DLR. In UPM viscous effects for arbitrary lifting bodies are predicted with a stripwise boundary layer analysis method, which compute flows along the spanwise segments. For non-lifting bodies like fuselages, a simplified boundary layer analysis method is utilized in the original UPM-version, which is based on local flow properties and the flat plate analogy. Flow separation is detected with simple flow separation criteria. In this paper, a more accurate boundary layer method proposed by Truckenbrodt (Refs. 8, 13, 14) is implemented. Truckenbrodt's method is based on a range of experiments executed by J. C. Rotta (Ref. 7), which are very comprehensive in this field. It was incorporated in UPM for helicopter fuselages. The aim of this method is to determine the friction coefficient on the fuselage surfaces and to estimate the flow separation areas more accurately. The Truckenbrodt boundary layer method for arbitrary non-lifting bodies is validated for a helicopter fuselage wind tunnel experiment and is applied to an air taxi type emergency deployment vehicle.

3. COMPUTATIONAL METHOD

3.1. Unsteady 3D Panel and Free-Wake Method (UPM)

DLR's unsteady panel and free-wake code UPM (Refs. 1, 15) supports the development process of helicopters. It is a research code initially meant for aeroacoustic simulations of rotorcraft, in particular for blade vortex interaction (BVI). It is currently being modernized and enhanced for the aerodynamics of complete helicopters (Ref. 5). UPM was used for many different components of the helicopter like isolated fuselage (Ref. 5), isolated rotor (Ref. 1), main-tail rotor interaction (Ref. 15), main and lateral rotor interaction (Ref. 19), propeller-wing and engine exhaust interaction (Ref. 16). In addition, it has been used for rotor blades' performance optimization (Ref. 20) and for investigating the effect of helicopter wakes on an obstacle (Ref. 9). UPM utilizes the velocity-based potential flow formulation with Neumann boundary conditions, based on the work of Hess and Smith (Ref. 4). UPM is able to calculate three-dimensional, incompressible, inviscid potential flows quickly and reliably.

Since viscous drag cannot be predicted using panel methods alone, the panel method is coupled with boundary layer methods. In UPM, structured panel grids are used to discretize lifting bodies like wings or rotors (Refs. 1,15), while unstructured grids are applied to simulate complex shaped non-lifting bodies, e.g. fuselages. In UPM, the standard stripwise integration of the boundary layer equations along grid lines is applied for structured grids. The viscous boundary layer calculation for unstructured surface panels is more demanding than for structured panels, since the boundary layer flow doesn't align with the grid lines. Most other panel codes extract stream lines on the body surfaces and compute the boundary layer along these streamlines. The boundary layer data are then mapped onto the fuselage surface. In UPM, in contrast to other methods, for unstructured grids an advancing front algorithm is applied to propagate boundary layer data along the surface (Ref. 5) in streamwise direction. The advantage of this approach is that no user interaction is required for the extraction of streamlines. Two approaches are available in UPM to predict boundary layers on unstructured surface grids: a flat plate analogy and the newly implemented method by Truckenbrodt.

3.2. Flat plate analogy

An often-used simplified approach for computing skin friction is the flat plate analogy. In this case all stagnation points are detected on the surface and the arc length in streamwise direction is propagated by the advancing front algorithm. A Reynolds number is computed based on the arc length and the local flow velocity. Now, an equation proposed by Schlichting for the flow about a flat plate is solved for the skin friction (Refs. 5, 6) (Eq.(1)).

$$c_f = [2\log_{10}(Re) - 0.65]^{-2.3}, \qquad Re < 10^9 \tag{1}$$

Simple empirical criteria are used to predict separation onset. Angle and Stratford criterions are obtainable for estimation the flow separation areas in UPM. According to the angle criterion, it is assumed that flow separation will occur if the angle between the local panel normal vector and the flow direction exceeds a certain critical value. The suggested angle for bluff bodies is 20 degrees (Ref 6). For flow separation estimation according to Stratford criterion the calculated factor $f_{stratford}$ (Eq. (2)) depends on the c_p and local Reynolds number Re. If this factor greater than the empirical value of 0.39 the flow separation occurs. If the factor is less than the value of 0.10 the reattachment of the flow is assumed: If a flow separation is detected, the skin friction coefficient set to zero. For more detailed description, the reader is referred to Ref. 5 and Ref. 11.

$$f_{stratford} = \frac{c_p\sqrt{s \cdot \frac{dc_p}{ds}}}{(10^{-6} \cdot Re)^{1/10}} \tag{2}$$

3.3. Truckenbrodt's boundary layer method

There are two calculation methods for turbulent boundary layers: integral and differential. The differential method has a higher calculation effort and larger storage space requirement than the integral method (Ref. 13). For this reason, an integral method was selected in this work.

Truckenbrodt's boundary layer method (Refs. 8, 13, 14) is an integral boundary layer method. It can be used for both planar and rotationally symmetric turbulent flows. It employs the calculated flow quantities to compute skin friction on each individual panel, and to identify flow separation.

The boundary layer can be calculated using the basic equations of momentum or mechanical energy. The variables of the momentum method are denoted with the index 2 and the energy method are denoted with the index 3. Truckenbrodt's boundary layer method uses the energy method (Refs. 8, 13). There are essential parameters that make the description of the boundary layer method easier: The boundary layer thickness δ and the velocity distribution of the flow U.

The boundary layer thicknesses δ are calculated using displacement thickness δ_1, momentum δ_2 and energy loss thicknesses δ_3. Detailed derivation of the formulas is shown in Schlichting (Ref. 8).

The local Reynolds number Re (Eq. (3)) is calculated by the boundary layer thicknesses δ, velocity distribution U and kinematic velocity ν .

$$Re_2 = \frac{\delta_2 \cdot U}{\nu} \qquad Re_3 = \frac{\delta_3 \cdot U}{\nu} \tag{3}$$

The shape parameters H_{12}, H_{23}, H_{32} are the ratio of the boundary layer thicknesses (Eq. (4)). They are dimensionless and they denote the velocity profile, which strongly depends on the pressure gradient of the external flow (Ref. 8).

$$H_{12} = \frac{\delta_1}{\delta_2} \qquad H_{23} = \frac{\delta_2}{\delta_3} \qquad H_{32} = \frac{\delta_3}{\delta_2} \tag{4}$$

The relations between the form factors H_{12} and H_{23} are approximated in Ref. 8 as given by the Eq. (5) and (6). The relation between H_{23} und H_{32} is as in Eq. (7).

$$H_{12} = \frac{4.65583 \cdot 10^{-2}}{\mathrm{x} - 7.05788 \cdot 10^{-1}} + 1.13303 \tag{5}$$

$$H_{23} = \frac{1.61239 \cdot 10^{-2}}{\mathrm{x} - 6.35881 \cdot 10^{-1}} + 5.10871 \tag{6}$$

$$H_{32} = 1/H_{23} \tag{7}$$

According to this procedure, the local Reynolds number Re_3 (Eq. (8)) is determined. E_3 is the integration constant (Eq. (9)) where x is the coordinate in the flow direction and it is dimensionless.

$$Re_3(x) = \left(\frac{1}{80 \cdot \nu} \frac{E_3(x)}{[U(x)]^{2\cdot(1+0.152)}}\right)^{1/(1+0.152)} \tag{8}$$

$$E_3(x) = E_3(x) + \int_{x_1}^{x} U^{3+2\cdot 0.152} dx \tag{9}$$

A modified shape parameter H is calculated with the parameters G and N, which are influence functions of the velocity distribution of the external flow (Eq. (10)-(12)).

$$H(x) = U(x) \cdot G(x) \cdot [N(x)]^{-1/4} \tag{10}$$

(11) $$G(x) = G(x_1) + \int_{x_1}^{x} U^{2(1+0.152)} dx$$

(12) $$N(x) = N(x_1) + 4 \cdot \int_{x_1}^{x} U^{2(1+0.152)+4} \cdot G^3 dx$$

The initial values of the integration constants for G and N are calculated in Eq. (13) and(14).

(13) $$G(x_1) = 80 \cdot \nu \cdot [H(x_1) \cdot U(x_1)^{1+2\cdot 0.152} \cdot Re_3(x_1)^{1+0.152})$$

(14) $$N(x_1) = \left[U(x_1) \cdot \frac{G(x_1)}{H(x_1)}\right]^4$$

The wall shear stress coefficients c_f (Eq. (15)) depends on the Reynolds number and the form factor.

(15) $$c_f = \frac{0.0245 \cdot (1 - 2.007 \cdot log H_{12})^{1.705}}{Re_2^{0.268}}$$

Truckenbrodt (Ref. 12, 13) calculated the wall shear stress with Re_3. The Reynolds numbers Re_2 and Re_3 are calculated the same since the coefficients required for calculating these numbers are the same. Therefore, exchanging the Reynolds number definitions do not cause any difference. Rotta (Ref. 7) and Walz (Ref. 17) present the conditions depending on the shape parameters when flow separation can occur in turbulent boundary layers. According to Rotta, turbulent flow separation occurs when the shape parameter H equals approximately 0.723, and according to Walz, when the shape parameter is between 0.723 and 0.761 (Ref. 8). On the contrary, Truckenbrodt (Ref. 13) suggests that flow separation occurs when the value of shape parameter H is less than or equal to 0.723.

3.4. Implementation of Truckenbrodt's method in UPM

Flow conditions and the velocity distribution are the input data for Truckenbrodt's boundary layer calculation.

In UPM, for each panel the flow variables such as local velocities are determined according to potential flow theory. The advancing front algorithm checks the flow direction for each unstructured panel. If the flow goes from a panel into all of its neighboring cells, this panel is defined as a stagnation point. Therefore, this surface panel has a velocity of approximately 0 m/s and a pressure coefficient of approximately 1. The stream arc length along a panel depends on the flow direction, which is given by the local flow velocity. Figure 1 shows three neighboring panels which are numbered 1, 2 and 3. It is assumed that the stream arc length of panel 1 and 3 are computed from a previous iteration of the advancing front algorithm, while the arc length of panel 2 is unknown. The interpolated velocities at the panel boundaries are shown with black arrows. The flux over the relative panel boundaries is depicted with orange arrows. The flux is determined by the multiplication of the length of the panel boundaries and the interpolated velocity component perpendicular to the panel boundaries. Then, the stream arc length along the panel 2 is computed based on the arc length of the neighbor panel with the largest incoming flux. In this case the incoming flux from panel 1 is greater than the incoming flux from panel 3, thus the arc length along panel 2 is calculated based on the known arc length of panel 1. The arc length is given by projecting the coordinates of panel centers 1 and 2 onto the normalized vector $\overrightarrow{v_{1\to 2}}$. In addition, all boundary layer data required by Truckenbrodt's method are computed from the known values in panels 1 and 2. The advancing front algorithm is iteratively repeated until the boundary layer data are computed for all surface panels.

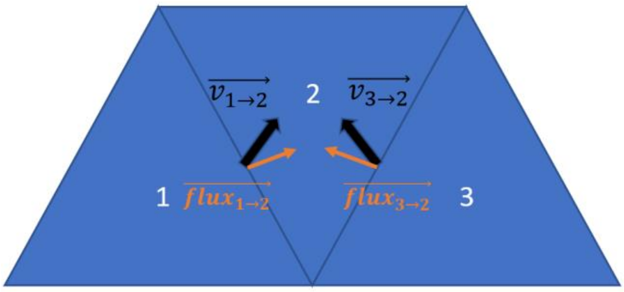

Figure 1: Flux direction of the neighboring panels

The skin friction coefficient c_f is calculated according to Truckenbrodt's wall shear stress c_f (Eq. (15)). Flow separation occurs, if the form factor H is smaller than a user provided critical value. In this work a form factor H=0.723, as recommended by Truckenbrodt and H=0.82 are used and compared. If the form factor is greater than 0.9 the flow is reattached. Due to the fact that UPM only calculates attached flow, the friction coefficient c_f is set to zero when the Truckenbrodt's separation criterion is met. The surface pressure coefficient c_p is corrected for separated flow areas and its value is set to zero.

4. TESTCASES & RESULTS

The newly implemented integral boundary layer method is first tested and validated with wind tunnel results obtained within DLR's Fast Rescue project. Later, the aerodynamic calculations of a medical personnel deployment vehicle will be presented.

4.1. Fast Rescue wind tunnel experiment

The DLR-internal project Fast Rescue seeks for new helicopter configuration designs, where next to other configurations a future rescue helicopter was designed. The power and flight envelope limitation are considered in the design. The wind tunnel experiment for the conventional helicopter fuselage featuring a streamlined body and V-tail was carried out in the DNW-NWB low-speed wind tunnel in Braunschweig (Figure 2, (Ref. 10)). The fuselage was fixed with a strut in the wind tunnel and it is scaled by 1 / 6 with respect to the potential full-scale vehicle. The original design employs a Fenestron-type tail rotor below the V-tail, which was replaced with a closed casing in the experiment. The components are created using a 3D printing process. Table 1 shows the measurement settings used for validation in this paper.

Figure 2: Wind tunnel components

Table 1: Measurement settings of Fast Rescue project in the wind tunnel.

Properties		
Mach number	0.205	
Reynolds number	$4.1 \cdot 10^6$	1/m l
Wind speed	70	m/s
Reference temperature	288	K

The numerical model features the fuselage, V-tail and the support strut, which are based on the original CAD geometry in CATIA of the wind tunnel model. An unstructured mesh with quadrilateral and triangular panels is used for the fuselage. A structured mesh with quadrilateral panels is used for the V-tail and the strut. The computational meshes are created with the Pointwise mesh generator. The meshes have around 20000 nodes (Figure 3).

The flow is considered fully turbulent for the fuselage; while being laminar and turbulent for the tail surfaces. The boundary layer analysis is performed firstly using the Truckenbrodt's boundary layer method and the flat plate analogy with separation Stratford criterion for the fuselage. Eppler's boundary layer method is used for tails and strut. Eppler is the standard setting for wings in UPM (Ref. 5). The results of the strut are not taken in account in the postprocessing.

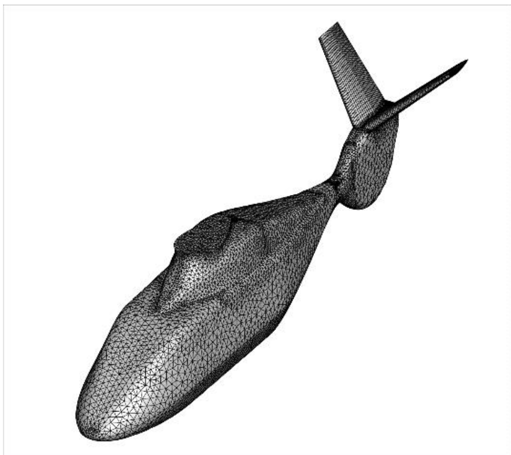

Figure 3: Mesh of Fast Rescue fuselage & tails

At first a polar was computed for the angle of attacks ranging from -15° to 15° with 2.5° steps. A comparison of the results using Truckenbrodt's boundary layer method and the flat plate analogy with Stratford criterion is shown for the surface pressure coefficients (Figure 4, Figure 5) and skin friction coefficients (Figure 6, Figure 7, Figure 8) for forward flight at the angle of attack of $\alpha = 0°$ and $\alpha = 15°$. Because there is a minimal difference, surface pressure coefficient is presented only for the case form factor H≤0.723 for Truckenbrodt's method. From the figures the stagnation point can be identified, which is on the nose of the fuselage. A symmetrical flow behavior can be observed from these figures. A positive angle of attack means that the flow is coming towards the bottom of the fuselage or the nose of the fuselage has moved upwards. With a positive angle of attack, the stagnation point was moved down and the suction area on the stabilizer increases. Truckenbrodt's boundary layer methods and the flat plate analogy with Stratford's criterion show very similar results. Minor differences between them are observed on engine cowling and fenestron.

There is a considerable area behind the rotor head, where the friction coefficient is almost zero. This is an area were flow separation occurs. Figure 6 and *Figure 7* show the Truckenbrodt's boundary layer methods with a form factor of H≤0.723 and H≤0.82. The latter value predicts flow separation more upstream and is larger than the recommended value by Truckenbrodt but has been calibrated to better match some of the experimental data used in this work. The separated flow areas increase with increasing form factor H value. Especially the separated flow areas on the rotor head and engine cowling are enhanced.

The Truckenbrodt's boundary layer methods and flat plate analogy with Stratford's criterion have salient differences in surface friction coefficients. At $\alpha = 0°$, the Stratford criterion shows larger separation areas at the rotor head and on the engine cowling side compared to the Truckenbrodt's method. The separated flow areas are spread out. The area of the separated flow at $\alpha = 15°$ is larger with the Stratford criterion. It is observed that there is separation especially in the tail rotor region. The Stratford criterion leads to earlier flow separation.

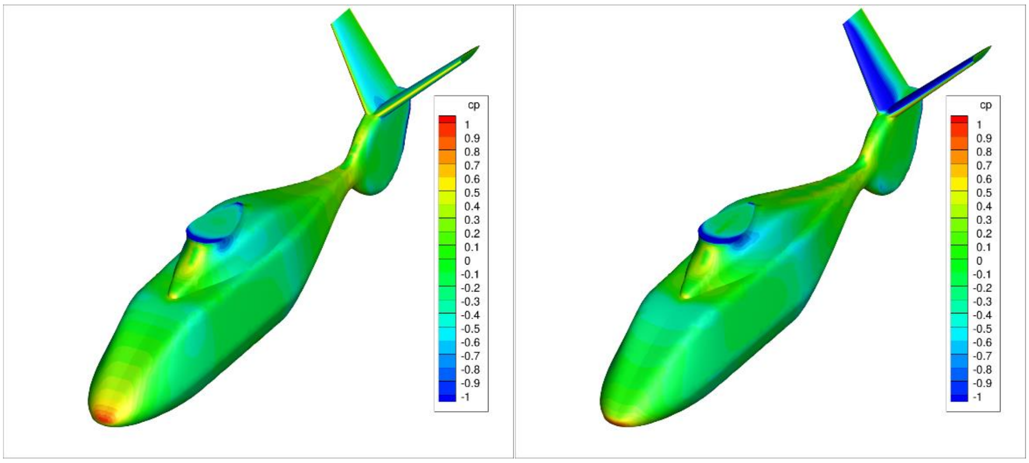

Figure 4: Surface pressure coefficient on UPM with Truckenbrodt's BL (H≤0.723) ($\alpha = 0°$ left; $\alpha = 15°$ right)

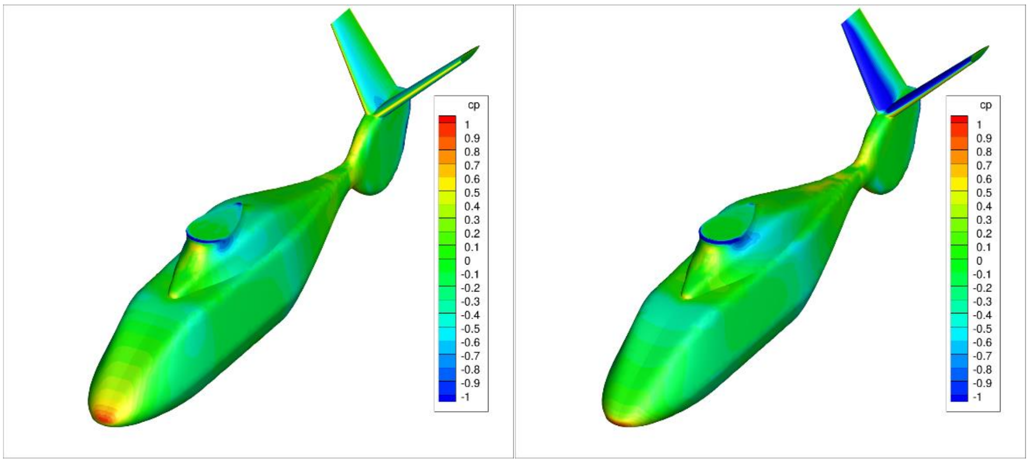

Figure 5: Surface pressure coefficient on UPM with flat plate analogy and Stratford's criterion ($\alpha = 0°$ left; $\alpha = 15°$ right)

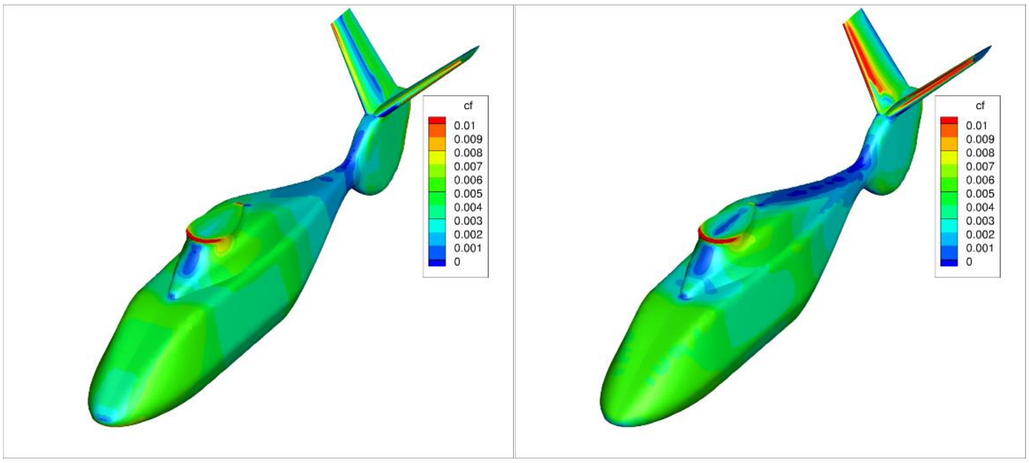

Figure 6: Skin friction coefficient on UPM with Truckenbrodt’s BL (H≤0.723) ($\alpha = 0°$ left; $\alpha = 15°$ right)

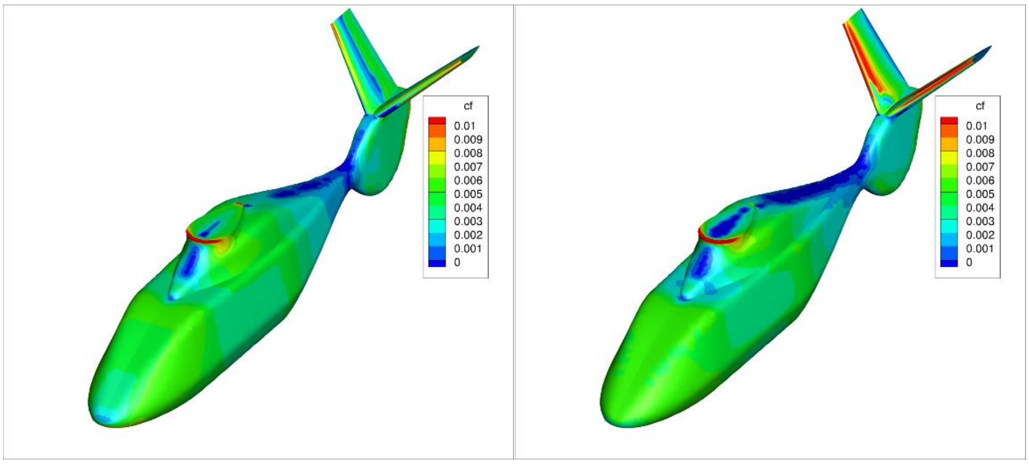

Figure 7: Skin friction coefficient on UPM with Truckenbrodt’s BL (H≤0.82) ($\alpha = 0°$ left; $\alpha = 15°$ right)

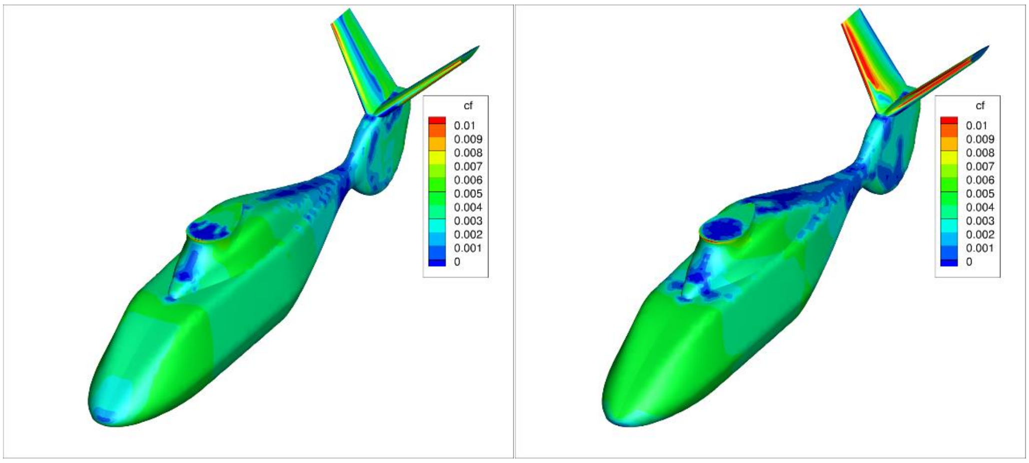

Figure 8: Skin friction coefficient on UPM with Stratford criterion ($\alpha = 0°$ left; $\alpha = 15°$ right)

Figure 9, Figure 10 and Figure 11 present the pressure coefficient c_p in the symmetry plane of the fuselage at three different angles of attack for Truckenbrodt’s boundary layer methods and with flat plate analogy including Stratford’s criterion. Red and green curves show the UPM top and bottom section results. Blue and black points represent wind tunnel top and bottom sensor results.

The Truckenbrodt methods coincide well with the experiment in the top section of the fuselage at $\alpha = -15$. But some deviation can be noticed on the engine cowling with Truckenbrodt's method with H$\leq$ 0.723. The reason for the deviation of the surface pressure coefficient on the bottom section is not known yet. Comparison with future CFD analysis should be carried out to explain this deviation. The flow detaches with H$\leq$ 0.82 on the bottom side of the engine cowling earlier.

At $\alpha = 0°$ the results of Truckenbrodt's method with H$\leq$ 0.723 show good agreement with the experiment. But there is earlier flow separation with H$\leq$ 0.82. The flow separation behind the rotor head on the top of the fuselage at $\alpha = 15$ has been already shown in Figure 6 and Figure 7. When flow separation occurs, the skin friction coefficients c_f and the surface pressure coefficients c_p are set to zero, which is also clearly seen in Figure 6 and Figure 7.

Using the Stratford criterion method, the flow was separated at $\alpha = -15°$ and $\alpha = 0°$ on the bottom section of the fuselage (Figure 11), but the flow presumably didn't separate for wind tunnel results. At $\alpha = 15°$, as shown in Figure *8*, the flow on the upper side of the fuselage was partially separated, which is also be seen in Figure 11 in the c_p distribution.

Overall, the Truckenbrodt's boundary layer method with H$\leq$ 0.723 provides more reasonably accurate results compared to the flat plate analogy with Stratford criterion. The agreement between numerical and experimental is good.

The drag (c_d), lift (c_l) and pitching moment (c_{my}) coefficients in dependency of the angle of attack are plotted in Figure 12. The flat plate analogy with Stratford criterion (UPM St) and Truckenbrodt's methods (H$\leq$ 0.723 and H$\leq$ 0.82) were compared with the experimental results.

The findings indicate that the drag coefficient c_d in UPM with Truckenbrodt's methods with positive angle of attack represents good alignment with the experiments. The larger form factor value H indicates better agreement of the drag friction with the experiment. On the other hand, the Stratford method shows a good agreement between -10° and 7.5° angle of attack with the experiment. Both methods establish that the numerical results differ from the experimental results as the angle of attack increases. The flat plate analogy with Stratford method depicts good alignment with the experiment for the lift coefficient results while the Truckenbrodt's method with H$\leq$ 0.723 deviates from the experiment. Truckenbrodt's method with H$\leq$ 0.82 has small deviation from the experiment and the flat plate analogy with Stratford results in the negative angle of attack. However, Truckenbrodt's method with H$\leq$ 0.723 shows better results than the flat plate-Stratford method for the pitching moment, especially at the negative angles of attack. In conclusion, both methods reveal an overall good alignment with the experiment and can be used for the forward flight.

The wind tunnel tests also included measurements for yaw angles of the configuration in the range from -15° to +15°.

Figure 13 and Figure 14 depict the surface pressure coefficient, Figure 15, Figure 16 and Figure 17 show skin friction coefficient at an angle of yaw of $\beta = 15°$ with Truckenbrodt's boundary layer methods and flat plate analogy with Stratford criterion. There is a minimal difference between two Truckenbrodt's boundary layer methods, surface pressure coefficient is presented only for the case form factor H$\leq$0.723. Because of the sideway flight, one side of the fuselage surface has higher pressure coefficients than the other side. A higher friction coefficient can be easily seen on the areas where the pressure coefficients are low because of high local velocities. The UPM results are in line with the expectations.

When the two methods are compared for the surface pressure coefficient, it can be seen from Figure 13 that Truckenbrodt's method shows bigger suction areas at the rotor head and at the tail-rotor area. But both methods show significant differences in skin friction coefficient results. The difference of the results due to this different computation can be seen in Figure 15, Figure 16 and Figure 17. As in the forward flight results, the Stratford method shows a dispersed separated flow area around the rotor head and behind the rotor head. At the same time, the suction area is larger on the tail-rotor. Truckenbrodt's method with H$\leq$ 0.82 shows the flow separation on the rotor head compared to Truckenbrodt's method with H$\leq$ 0.723.

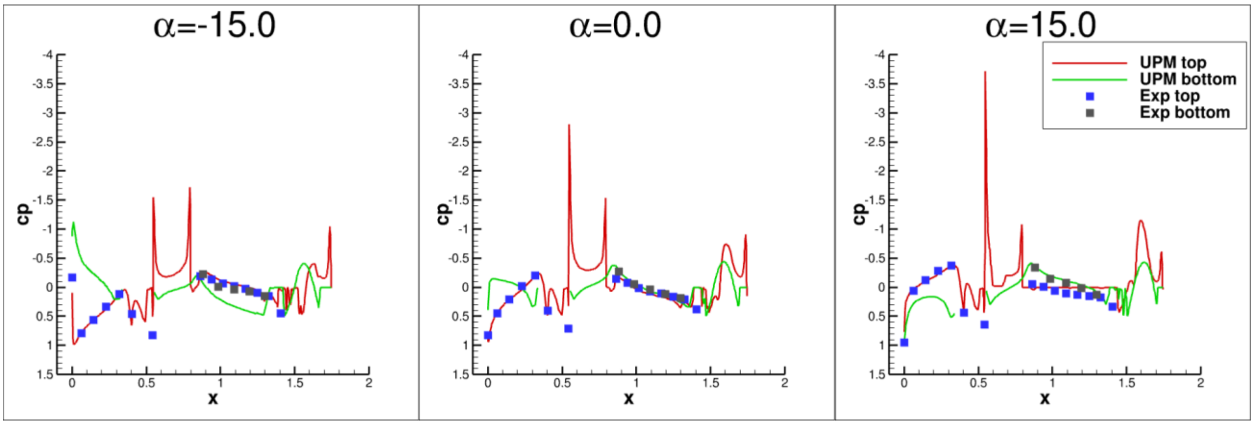

Figure 9: Surface pressure coefficient on UPM (Truckenbrodt (H≤0.723)) and Experiment in center cross section in dependency of angle of attack

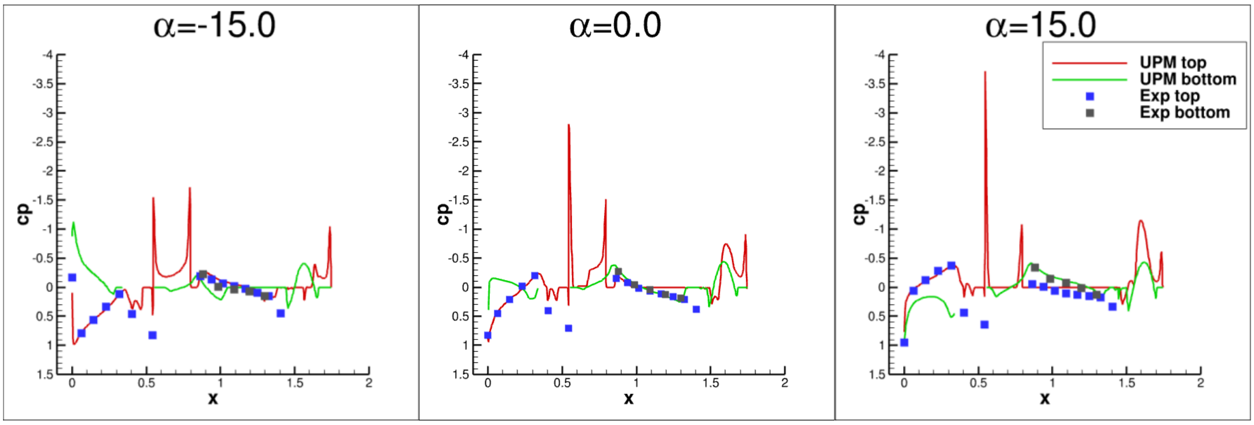

Figure 10: Surface pressure coefficient on UPM (Truckenbrodt (H≤0.82)) and Experiment in center cross section in dependency of angle of attack

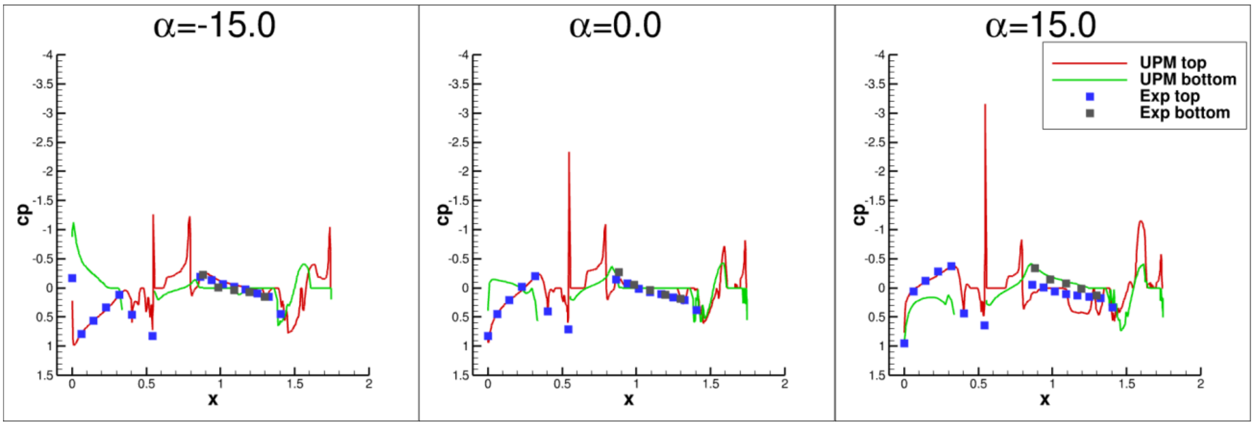

Figure 11: Surface pressure coefficient on UPM (Stratford) and Experiment in center cross section in dependency of angle of attack

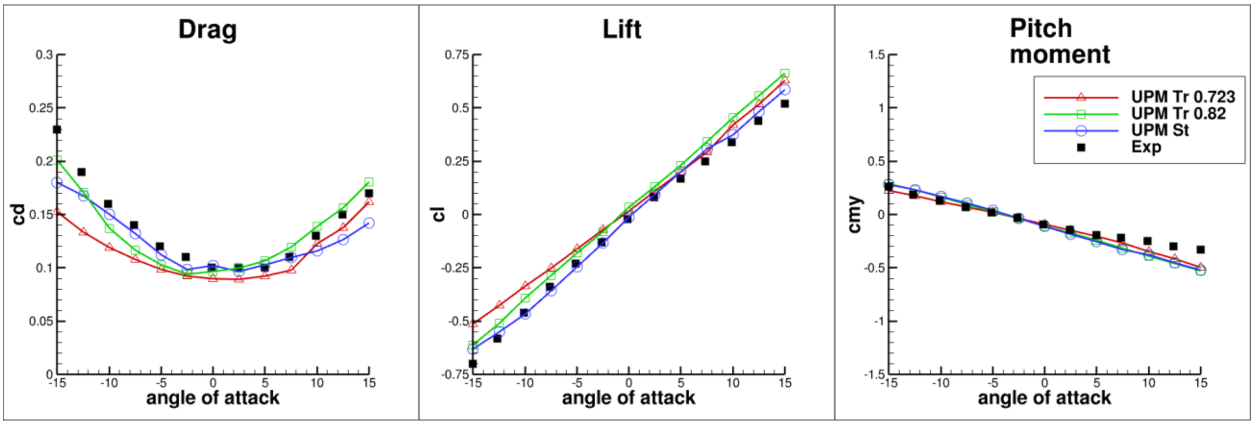

Figure 12: Drag, lift and pitch moment coefficients on UPM and Experiment in dependency of angle of attack

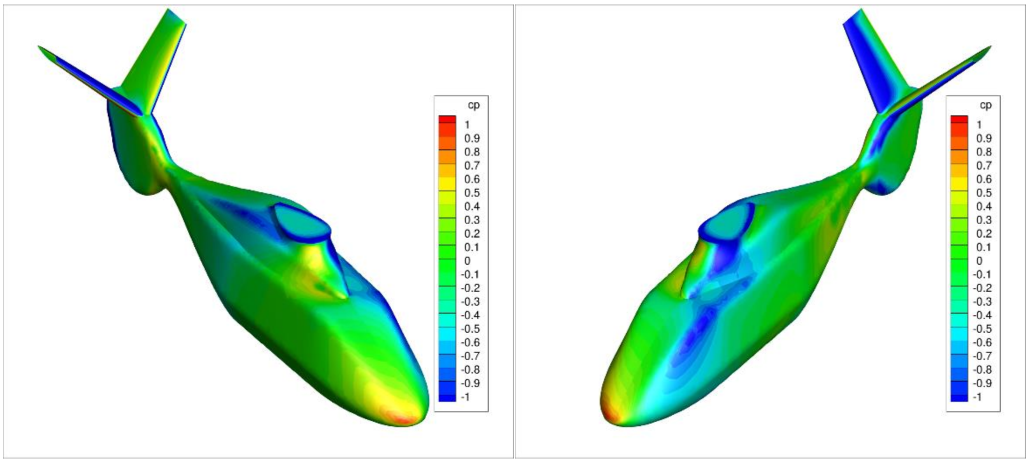

Figure 13: Surface pressure coefficient at $\beta = 15°$ in Truckenbrodt BL (H≤0.723)

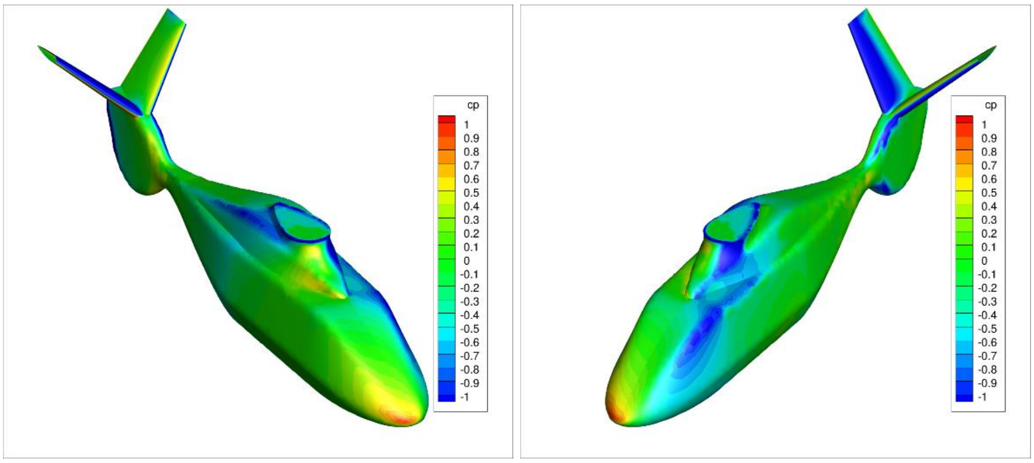

Figure 14: Surface pressure coefficient at $\beta = 15°$ in flat plate analogy with Stratford criterion

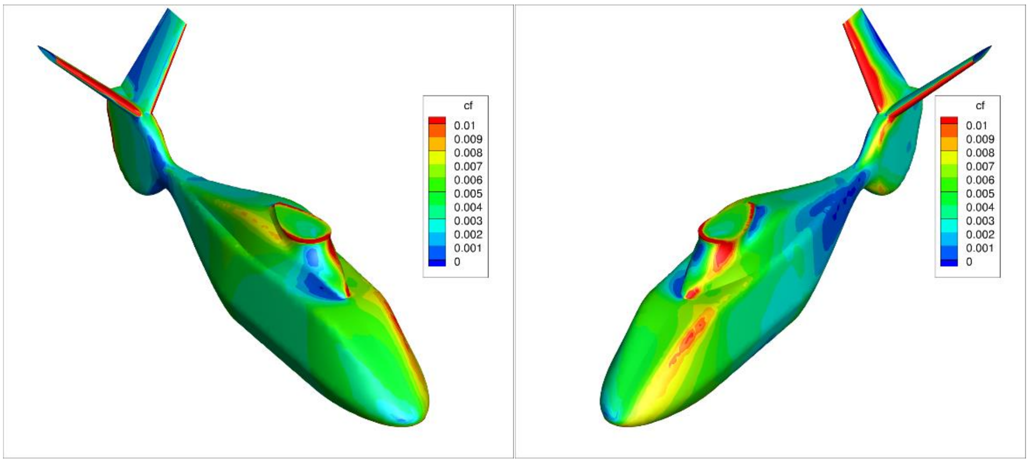

Figure 15: Skin friction coefficient on UPM at $\beta = 15°$ by Truckenbrodt BL (H≤0.723)

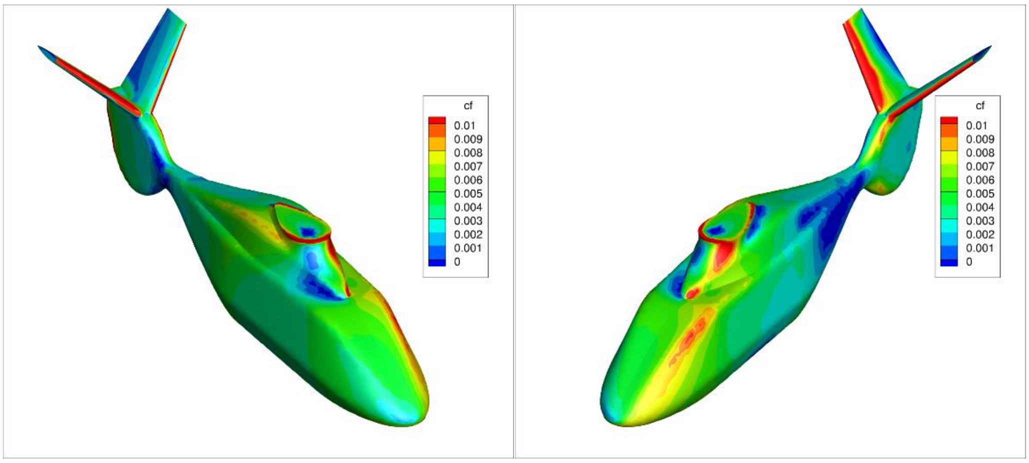

Figure 16: Skin friction coefficient on UPM at $\beta = 15°$ by Truckenbrodt BL (H≤0.82)

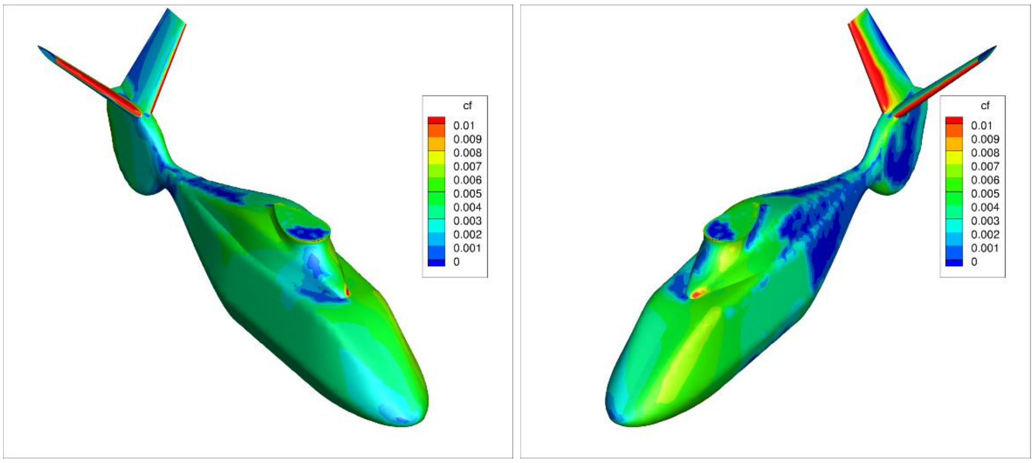

Figure 17: Skin friction coefficient on UPM at $\beta = 15°$ by flat plate analogy with Stratford criterion

Figure 18, Figure 19 and Figure 20 present the pressure coefficient c_p in the symmetry plane of the fuselage at three angles of yaw $\beta = 0°,\ 5°, 15°$ simulated with Truckenbrodt's boundary layer methods and flat plate analogy with Stratford criterion. Only positive angles are plotted because the positive and negative yaw angles have the same behavior due to the symmetry of the fuselage. As seen in the previous figures, with the Truckenbrodt's boundary layer method, flow separation is not seen behind the rotor head at $\beta = 15°$. At a lower angle of $\beta = 5°$, flow separation is not observed. With Stratford criterion, flow separation was observed behind the rotor head in all three cases. The surface pressure coefficient c_p in UPM in the center section shows a good agreement with the experiment with Truckenbrodt's boundary layer methods. The force coefficients (drag (c_d), lift (c_l) and lateral (c_s)) and moment coefficients (roll (c_{mx}), pitch (c_{my}) and yaw (c_{mz})) in dependency of the angle of yaw are plotted in Figure 21 and Figure 22. In these figures, Truckenbrodt's boundary layer methods and flat plate analogy with Stratford criterion are compared with the experimental results. The lift force coefficient of the Stratford criterion shows a better performance than the Truckenbrodt's boundary layer methods and the results are closer to the experiment. However, this method is quite insufficient for the drag force coefficient. Observation of early flow separation may be considered as the reason for this. Truckenbrodt's boundary layer method with H$\leq$ 0.82 has larger drag force coefficients compared to with H$\leq$ 0.723. Truckenbrodt's boundary layer methods and the flat plate analogy with Stratford criterion show similar results in lateral force coefficient and moment coefficients. Both force and moment coefficients have symmetrical behavior with respect to the angle of yaw. The agreement between the numerical results and the experiment is good for force and moment coefficients. In conclusion, the validation of UPM with Truckenbrodt's boundary layer method shows that the approach is an effective way of calculating the drag coefficient of the fuselage with good accuracy.

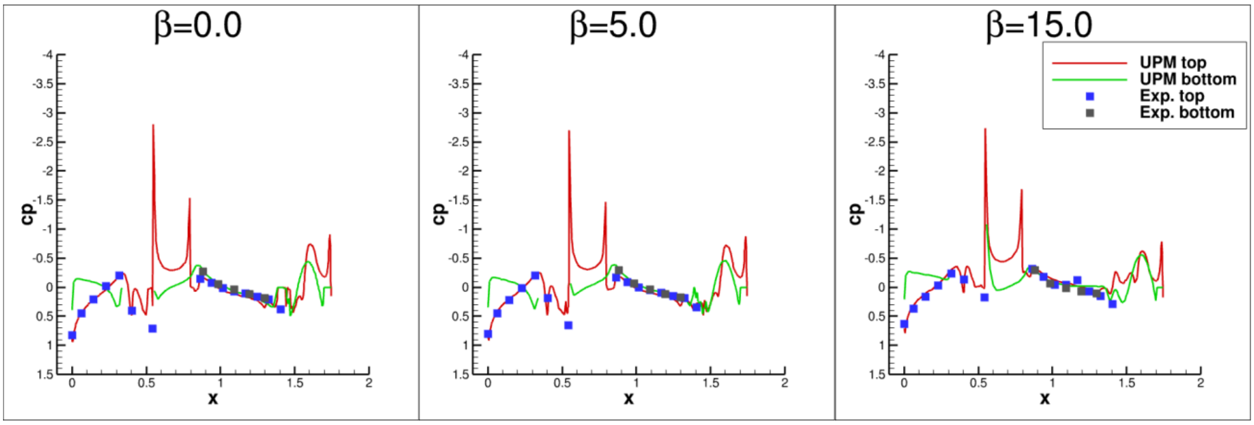

Figure 18: Surface pressure coefficient on UPM (Truckenbrodt (H≤0.723)) and Experiment in center cross section in dependency of angle of yaw

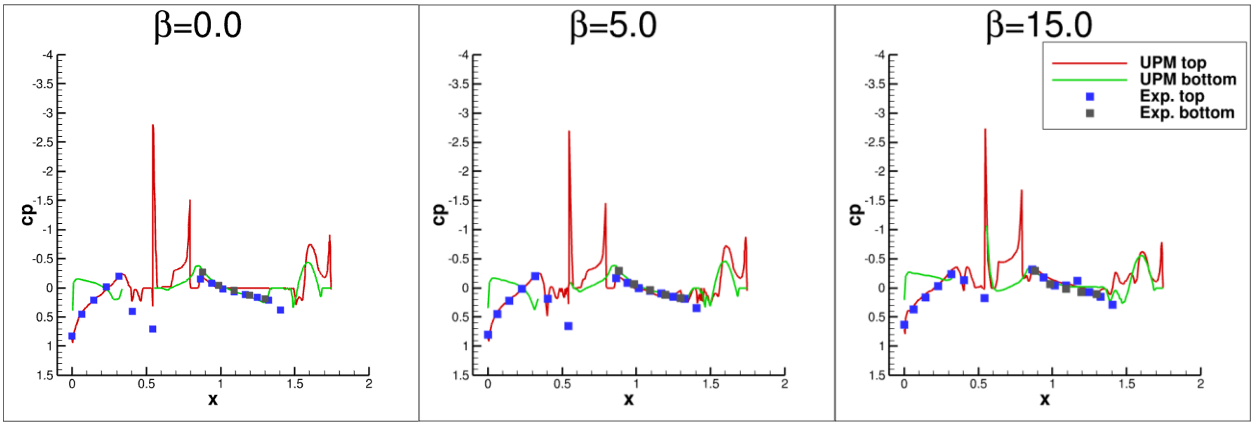

Figure 19: Surface pressure coefficient on UPM (Truckenbrodt (H≤0.82)) and Experiment in center cross section in dependency of angle of yaw

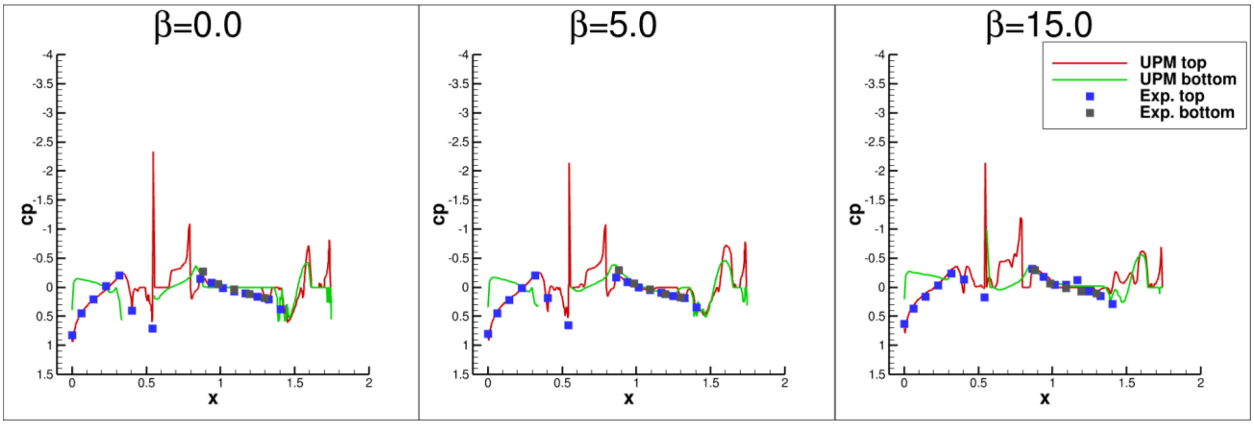

Figure 20: Surface pressure coefficient on UPM (Stratford) and Experiment in center cross section in dependency of angle of yaw

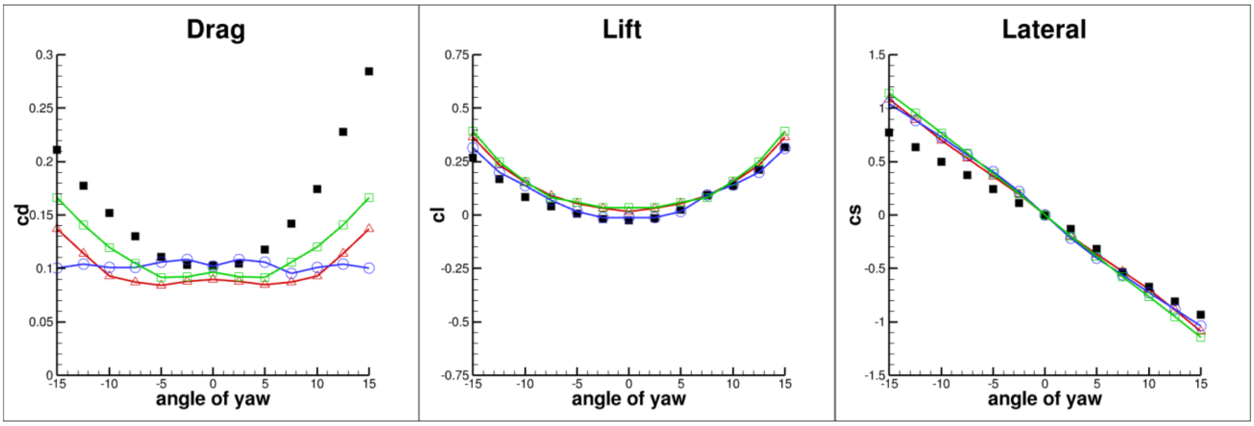

Figure 21: Force coefficients on UPM and experiment in dependency of angle of yaw

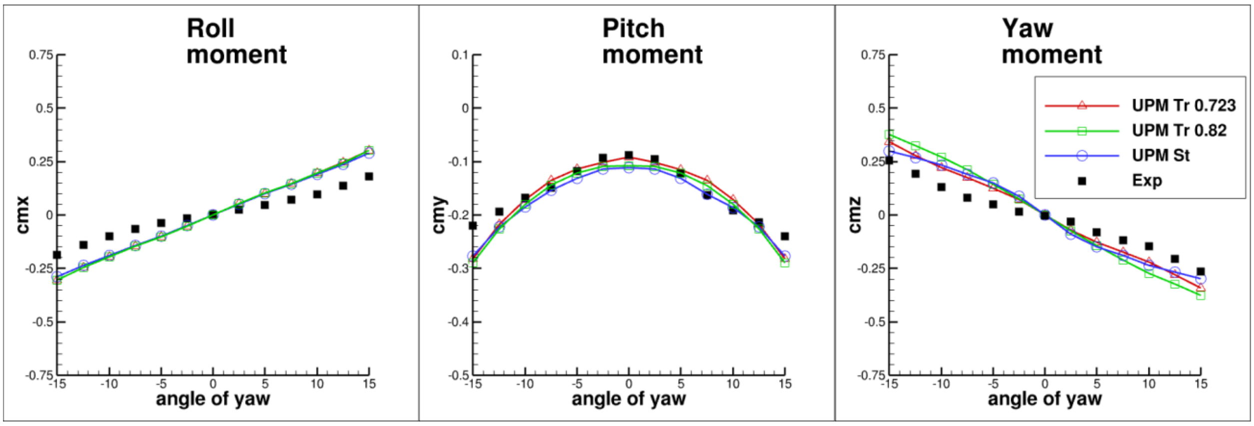

Figure 22: Moment coefficients on UPM and experiment in dependency of angle of yaw

4.2. Medical personnel deployment vehicle

As an application example, UPM was used to simulate the aerodynamics of a medical personnel deployment vehicle similar to an air taxi. The configuration is the outcome of a preliminary design study involving several DLR institutes using DLR's rotorcraft design environment IRIS (Integrated Rotorcraft Initial Sizing) (Ref. 18). For the UPM simulations, the required surface meshes for the air taxi were automatically created from the predesign data stored in the CPACS (Common Parametric Aircraft Configuration Scheme) data format (Ref. 2). It is an XML based format for describing aircraft configurations. The air taxi configuration has 4 main rotors, 2 pusher propellers and 6 booms (Figure 23). The concept was constructed for 2 passengers. Initial design weight is around 1 ton. The rotors are powered electrically. The rotor blades have a fixed pitch. Table 2 shows the flow condition of the preliminary design of the air taxi.

Figure 23: Medical personnel deployment vehicle

For the initial assessment of the configurations UPM was applied to compute polars for the isolated fuselage. Thus, the lifting rotors and the pusher propellers were not considered in the following calculation using UPM. The geometry consists of the fuselage and the six booms as shown in Figure 24. A structured mesh was used for meshing the fuselage and the booms. The booms are calculated as lifting surfaces. The meshes have around 15000 nodes. UPM was applied with Truckenbrodt's boundary layer methods (H≤ 0.723. and H≤ 0.82) and is compared with the flat plate analogy with Stratford criterion.

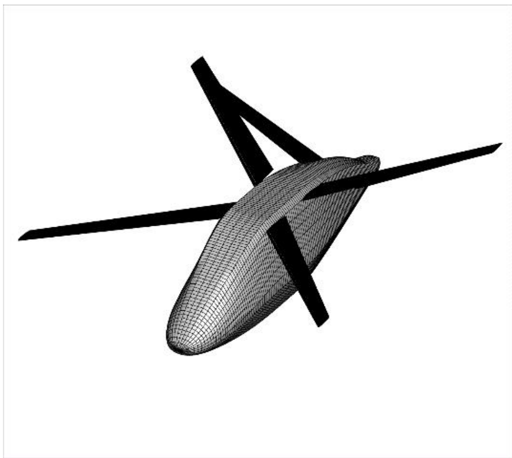

Figure 24: Medical personnel deployment vehicle in UPM

Table 2: Settings of medical personnel deployment vehicle

Properties		
Reynolds number	$2.8 \cdot 10^6$	1/m l
Wind speed	~ 42	m/s
Reference temperature	273	K

The study focuses on surface pressure, force and moments coefficients. The computations cover an angle of attack and an angle of yaw range between -15° and 15° with 2.5° steps for subsonic flow. Because no experimental results are available, the results are only shown for UPM.

Figure 25 and Figure 26 show the effect of increasing the angle of attack on the surface pressure coefficient with Truckenbrodt's boundary layer method and flat plate analogy with Stratford criterion. There is a minimal difference between the two Truckenbrodt's boundary layer methods. Therefore, the surface pressure coefficient is presented only for the case form factor H≤0.723. The stagnation point at $\alpha = 0°$ is on the nose of the fuselage. With a positive angle of attack $\alpha = 15°$, the stagnation point moves down and the suction areas on the booms increase. Both methods show the similar surface pressure coefficients.

Figure 27 illustrates the force and moment coefficients for a range of angle of attack. The difference between the three methods can only be seen in the drag coefficients. The outcomes are reasonable.

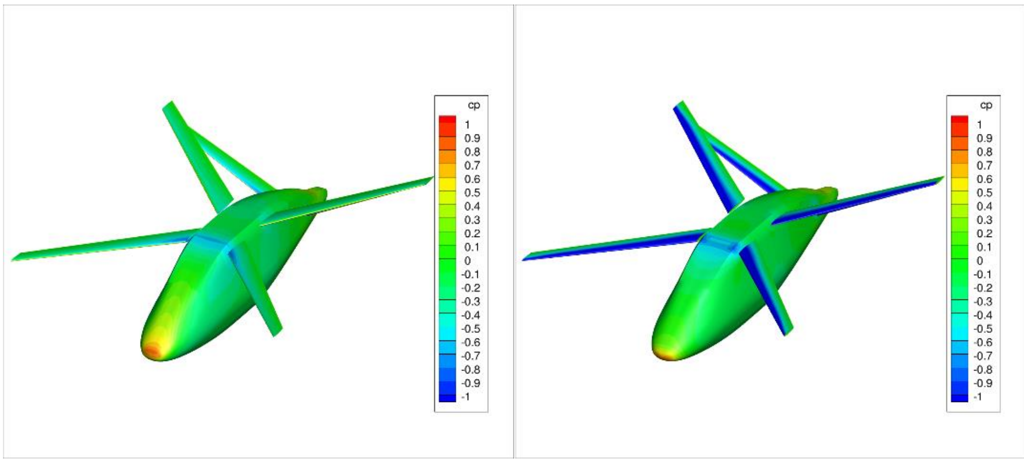

Figure 25: Surface pressure coefficient on UPM Truckenbrodt (H≤0.723) for the air taxi ($\alpha = 0°$ left; $\alpha = 15°$ right)

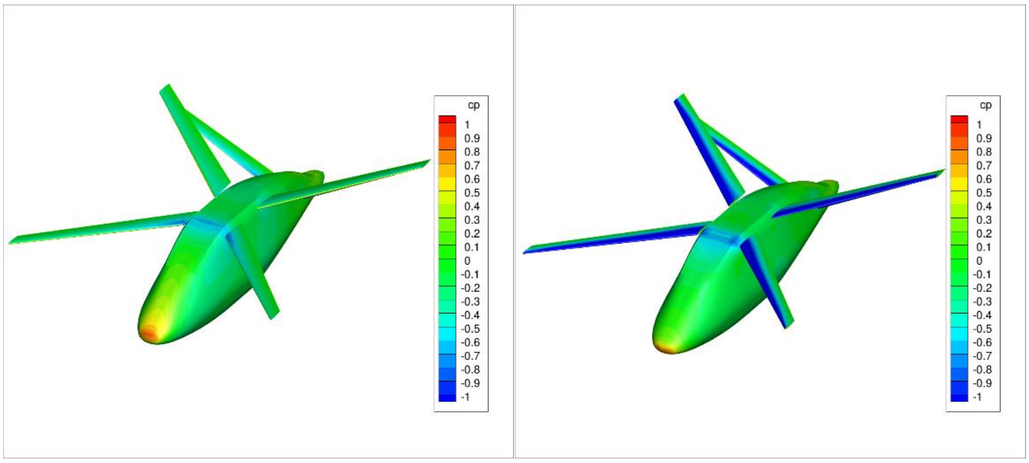

Figure 26: Surface pressure coefficient on UPM Stratford for the air taxi ($\alpha = 0°$ left; $\alpha = 15°$ right)

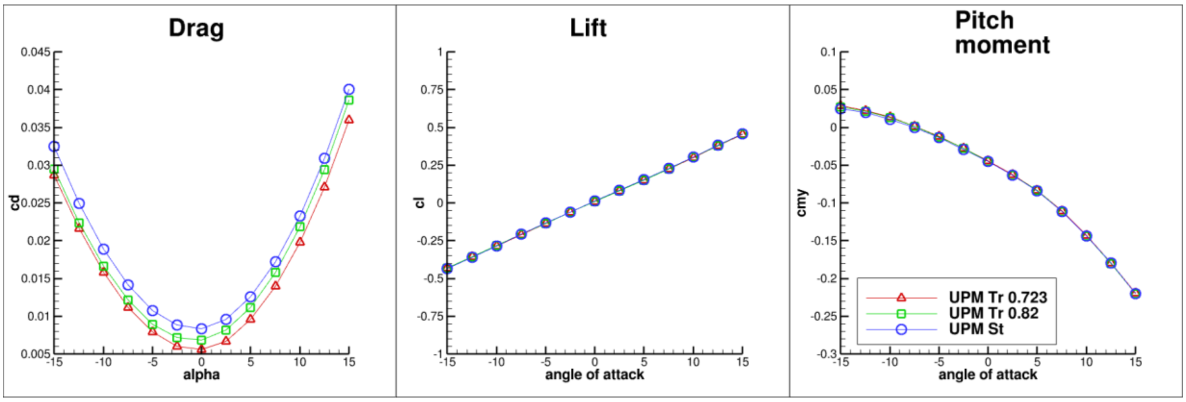

Figure 27: Drag, lift and pitch moment coefficients on UPM in dependency of angle of attack for the air taxi

Figure 28 and Figure 29 present the surface pressure coefficient at an angle of yaw of $\beta = 15°$ with Truckenbrodt's boundary layer method and flat plate analogy with Stratford criterion. As there is only a minimal difference between the two Truckenbrodt's boundary layer methods, surface pressure coefficient is presented only for the case using form factor H≤0.723. Because of the sideway flight, one side of the fuselage surface has higher pressure coefficient than and the other side. These UPM results are in line with the expectations. Figure 30 and Figure 31 depict the force coefficients and moment coefficients in dependency of the angle of yaw with the three methods. Both force and moment coefficients have symmetrical behavior with respect to the angle of yaw. Drag and lift coefficients with Truckenbrodt's boundary layer method of H≤0.82 and flat plate analogy with Stratford criterion show similar behavior. The differences between the methods are very small for other results. In conclusion UPM results are reasonable.

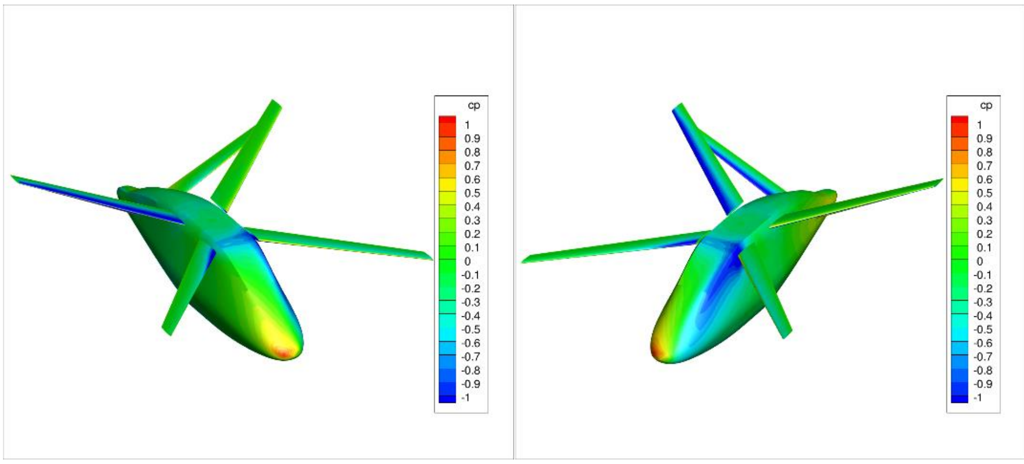

Figure 28: Surface pressure coefficient on UPM Truckenbrodt (H≤0.723) for the air taxi at $\beta = 15°$

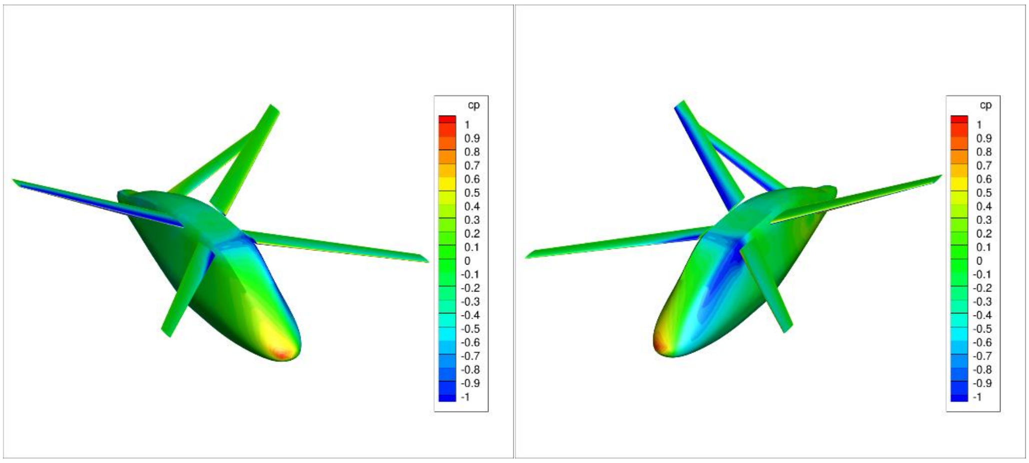

Figure 29: Surface pressure coefficient on UPM Stratford for the air taxi at $\beta = 15°$

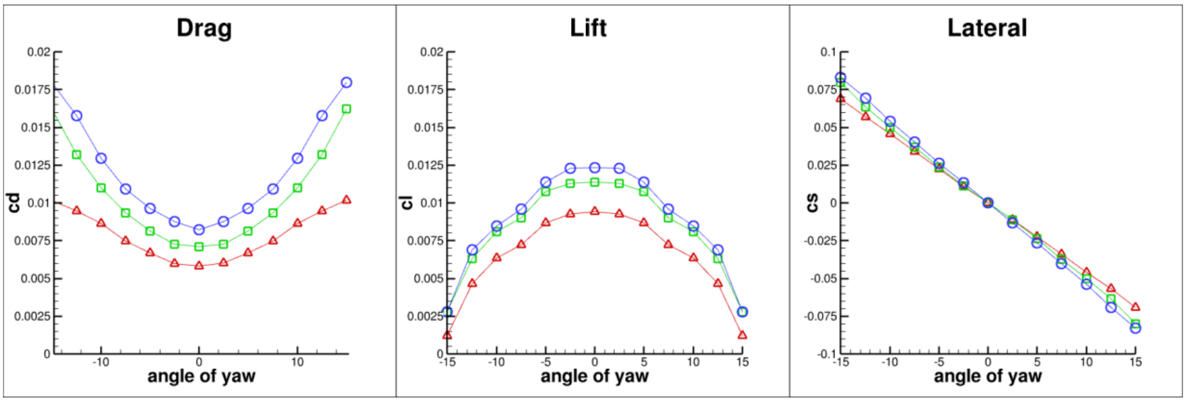

Figure 30: Force coefficients on UPM in dependency of angle of yaw for the air taxi

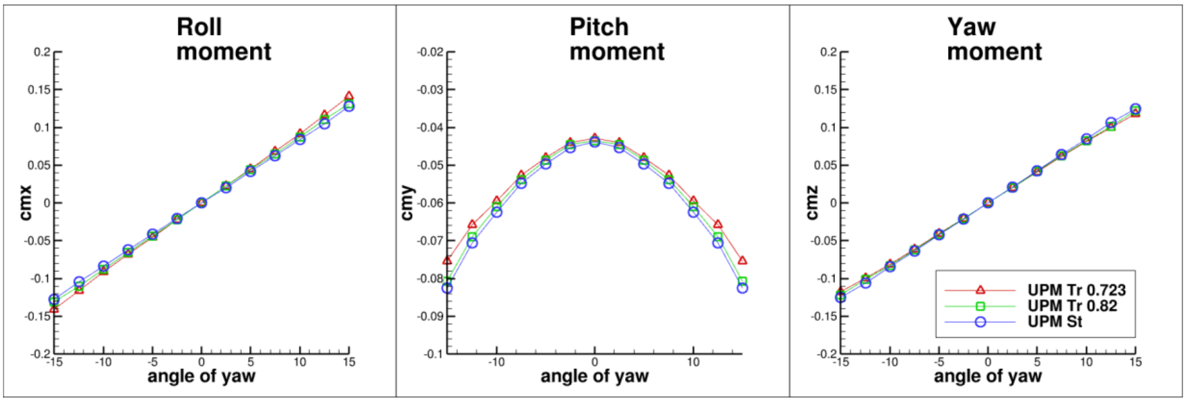

Figure 31: Moment coefficients on UPM in dependency of angle of yaw for the air taxi

5. CONCLUSIONS

In this paper the panel-free wake method UPM was extended with Truckenbrodt's boundary layer methods for predicting the viscous flow for non-lifting bodies. The newly implemented method is compared with the simpler flate plate analogy with Stratford's separation criterion. Both methods are validated for the helicopter fuselage of DLR's Fast Rescue project. After validation the Truckenbrodt's boundary layer methodology is applied for the prediction of the flow about a generic medical personnel deployment vehicle. The main findings are:

1. The predicted fuselage surface pressure coefficients and as well as forces and moments agree well with the wind tunnel results in forward flight with both methods.
2. Predicted areas with flow separations are more reasonable with the Truckenbrodt's boundary layer method compared to using Stratford's separation criterion.
3. Truckenbrodt's boundary layer method shows better agreement than Stratford criterion with the wind tunnel results in the side-slip flight for drag force coefficients.
4. The critical form factor H=0.723 used in Truckenbrodt's method to detect flow separations gives good results for the pressure distributions, while results using a fom factor H=0.82 agree better with measured loads.
5. Applications to a medical personnel deployment vehicle gives also reasonable results.
6. In all simulations the Truckenbrodt's boundary layer method worked resilient and reliably.
7. UPM code is a useful tool for aerodynamic helicopter simulation and it is a valuable for fast analysis and preliminary design.

In the future, UPM will be also compared to CFD simulations for the same configurations using CODA, the next generation CFD solver commonly developed by Airbus, DLR and ONERA. This will provide additional information about the accuracy of UPM results.

More advanced methods for separated flows will be implemented into UPM. Flow simulations of the medical personnel deployment vehicle in UPM will be calculated including the lifting rotors and pusher propellers.

Author contact:

Hilal Inac hilal.inac@dlr.de

Thorsten Schwarz thorsten.schwarz@dlr.de

6. REFERENCES

1. Ahmed, S. R. and Vidjaja, V. T., "Unsteady Panel Method Calculation of Pressure Distribution on BO105 Model Rotor Blades," *Journal of the American Helicopter Society*, Vol. 43, Sept. 1997, pp. 47-56.
2. Alder, M., Moerland, E., Jepsen, J. and Nagel, B., "Recent Advances in Establishing a Common Language for Aircraft Design with CPACS," Aerospace Europe Conference 2020, Bordeaux, France, 2020.
3. Cebeci, T., Mosinskis, G. J., and Smith, A. O., "Calculation of Separation Points in Incompressible Turbulent Flows,". *J. Aircraft*, Vol. 9, June 1972, pp. 618-624.

4. Hess, J., and Smith, A., "Calculation of potential flow about arbitrary bodies,". *Progress in Aerospace Sciences,* Vol. *8*, 1967, pp. 1-138.

5. Kunze, P., “A panel free-wake code with boundary layer method for helicopter simulations,” Paper ERF2019-0114, 45th Europaen Rotorcraft Forum, Warsaw, Poland, 17-20 Sept. 2019.

6. Kunze, P., “Approximate Boundary Layer Methods for a Fast Mid-Fidelity Aerodynamics Code for Helicopter Simulations,” STAB/DGLR Symposium 2020, NNFM 151, pp. 376-386, 2021.

7. Rotta, J. C, "Vergleichende Berechnungen von turbulenten Grenzschichten mit verschiedenen Dissipationsgrenzen," Ing. Arch. 38, pp. 212-222, 1969.

8. Schlichting, H.*, Grenzschicht-Theorie, 8. Auflage*, Karlsruhe, 1982, Chapter 22.

9. Schmid, M., “Simulation of Helicopter Aerodynamics in the Vicinity of an Obstacle using a Free Wake Panel Method,” 43rd Europaen Rotorcraft Forum, Mailand, Italy, 12-15 Sept. 2017.

10. Schneider, O., Mainz, H., Brehl, E., Henseleit-Wieser, S. and van der Wall, B. G., „Development of a new medium size helicopter wind tunnel model,” 50th Europaen Rotorcraft Forum, Marseille, France, 10-12 Sep. 2024.

11. Stratford, B. S., "The prediction of separation of the turbulent boundary layer,". *Journal of Fluid Mechanics*, Vol 5, 1959, pp.1-16.

12. Truckenbrodt, E., *Strömungsmechanik*; Berlin/Heidelberg/New York, 1968

13. Truckenbrodt, E., "Neuere Erkenntnisse über die Berechnung von Strömungsgrenzschichten mittels einfacher Quadraturformeln, Teil I,". Ingenieur-Archiv 43, 1973, pp. 9-25

14. Truckenbrodt, E., ”Neuere Erkenntnisse über die Berechnung von Strömungsgrenzschichten mittels einfacher Quadraturformeln, Teil II,". Ingenieur-Archiv 43, 1974, pp. 136-144.

15. Yin, J. P. and Ahmed, S. R., “Helicopter Main-Rotor/Tail-Rotor Interaction,” *Journal of the American Helicopter Society*, Vol. 4, July 2000, pp. 293-302.

16. Yin, J. P., Stuermer, A. and Aversano, M., “Aerodynamic and Aeroacustic Analysis of Installed Pusher-Propeller Aircraft Configurations,” *Journal of Aircraft*, Vol. 49, Sep.-Oct. 2012, pp. 1423-1433.

17. Walz, A. and Braun, G., *Strömungs- und Temperaturgrenzschichten*, Karlsruhe, 1966.

18. Weiand, P., Buchwald, M., and Schwinn, D. (2019). "Process Development for Integrated and Distributed Rotorcraft Design,". *Aerospace,* Feb. 2019

19. Wentrup, M., Yin, J., Kunze, P., Streit, T., Wendisch, J-H., Schwarz, T., Pinacho, J-P., Kicker, K. and Fukari, R., "An overview of DLR compound rotorcraft aerodynamics and aeroacustics actvities within the CleanSky2 NACOR Projects," AHS International 74th Annual Forum & Technology Display, Phoenix, Arizona, USA, May 14-17 2018.

20. Wilke, G., "Aerodynamic Optimization of Helicopter Rotor Blades using Variable Fidelity Methods," Phd. Thesis TU Braunschweig,Germany, March 2017.

7. CLASSIFICATION & COPYRIGHT